Ocean Modelling 74 (2014) 53–59

Contents lists available at ScienceDirect

Ocean Modelling

journal homepage: www.elsevier.com/locate/ocemod

Short communication

Tide-induced flow signature in rip currents on a meso-macrotidal beach

Nicolas Bruneau [a,*], Xavier Bertin [b], Bruno Castelle [c], Philippe Bonneton [c]

[a] Risk Management Solutions Ltd., Peninsular House, 30 Monument Street, London EC3R 8NB, UK
[b] UMR 7266 LIENSS CNRS, Université de La Rochelle, Institut du Littoral et de l'Environnement, 2 rue Olympe de Gouges, 17 000 La Rochelle, France
[c] UMR 5805 EPOC CNRS, Université Bordeaux 1, Talence F-33405, France

ARTICLE INFO

Article history:
Received 25 June 2013
Received in revised form 25 September 2013
Accepted 16 December 2013
Available online 25 December 2013

Keywords:
Rip current
Tide
Asymmetry
Modelling
Meso-macrotidal
Surf zone

ABSTRACT

On rip-channelled beaches, intense rip currents are driven by waves due to alongshore variations in breaking-induced wave energy dissipation. This study addresses for the first time the potential development of tidal currents superimposed onto the wave-driven circulation. This phenomenon is observed on a rip-channelled meso-macrotidal beach (Biscarrosse, SW France). Field measurements show 20 to 45% stronger mean rip velocities during ebb than during flood. Numerical experiments reveal that this asymmetry is the signature of tidal currents developing over the rip channel morphology. This asymmetry is found to increase roughly linearly with increasing tidal range. These results are significant to beach safety and lifeguarding and stimulate further numerical exercises.

1. Introduction

Surfzone sandbars are ubiquitous patterns in the sand along wave-exposed coasts. Sandbars often display remarkable alongshore periodic undulations in both their depth and cross-shore position referred to as crescentic sandbars or bar and rip systems. On these rip-channelled beaches, rip currents (narrow seaward-flowing jets) are driven by alongshore variations in bathymetrically-controlled wave breaking (Bonneton et al., 2010), with rip velocity fluctuating on timescales of the order of 1 min (infragravity motions, MacMahan et al., 2004a) and 10 min (Very Low Frequency motions, VLFs, MacMahan et al., 2004b). These topographically-controlled rip currents are one of the most deadly coastal hazards (Scott et al., 2011) and have a significant impact on transport and dispersion of pollutants, nutrients and tracers (Reniers et al., 2009, 2010; Shanks et al., 2010) and thus to the overall coastal ecosystem.

Over the last decades, scientists have been working to improve our understanding of topographically-controlled rip currents through a variety of techniques including field (e.g., Brander, 1999; MacMahan et al., 2004a; Bruneau et al., 2009; Austin et al., 2010) and laboratory (e.g., Haller and Dalrymple, 2001; Kennedy and Thomas, 2004; Castelle et al., 2010) experiments, video imaging systems (e.g., Holman et al., 2006; Turner et al., 2007) and mathematical and numerical modelling (e.g., Reniers et al., 2009; Castelle et al., 2006; Bruneau et al., 2011). In the field, for low- to moderate-energy wave conditions, tidal elevation is found to dictate occurrence of rip current activity. In most studies, increasing rip current activity occurs with decreasing tidal elevation resulting in maximum rip current intensity near low tide (e.g., Brander, 1999; MacMahan et al., 2006). Other studies noticed maximum rip current intensity between low and mid tide for low- to moderate-energy wave conditions (e.g., Brander and Short, 2000; Castelle et al., 2006; Bruneau et al., 2009; Austin et al., 2010, 2013) and rip current likely not flowing at high tide. In addition, on the SW coast of France, Castelle et al. (2006) and Bruneau et al. (2009) observed that the occurrence of maximum rip current intensity moves closer to high tide with increasing incident wave energy. Recently, Austin et al. (2013) observed the presence of net tidal currents in the alongshore direction on a macro-tidal beach. These authors noted maximum tide currents occurring around mid tide, when the maximum rip currents occur on the side of the low tide. Overall, the common perception of rip currents in tidal environments is that tide acts mainly as a change in water level. This means that, for a given wave condition and tidal elevation, rip current intensity is the same during ebb and flood. Yet, a more detailed examination of the rip current data in Bruneau et al. (2009) suggests that this is not exactly the case as substantially larger rip current intensities were measured during ebb than during flood. This corroborates qualitative lifeguard observations on this stretch of the French coast which suggest that, during low-energy wave conditions, rip

* Corresponding author. Tel.: +44 2074447730.
E-mail address: nicolas.bruneau@rms.com (N. Bruneau).

1463-5003/$ - see front matter © 2013 Elsevier Ltd. All rights reserved.
http://dx.doi.org/10.1016/j.ocemod.2013.12.002

currents are more efficient in pulling swimmers away during ebb than during flood. Accordingly, it is worth testing the hypothesis that tide-induced currents on wave-exposed rip-channelled beaches are significant.

In Section 2, the study area and the field experiments as well as the modelling strategy are described. Section 3 presents field evidence of the tidal signature in rip current velocity data at Biscarrosse Beach (Bruneau et al., 2009) and model application to investigate the influence of the hydrodynamic forcing (tides and wave conditions) on rip current flow asymmetry. A discussion on the impact of this flood/ebb asymmetry in rip currents is presented in Section 4.

2. Data and method

2.1. Study site and data collection

The Aquitanian coast is a wave-dominated, high-energy, meso- to macrotidal environment exhibiting a strongly alongshore non-uniform and dynamic double sandbar system (Castelle et al., 2007). The outer and inner bars exhibit most of the time crescentic patterns and a transverse bar and rip morphology, respectively. Biscarrosse Beach is located at about 10 km southward of the Arcachon Lagoon Inlet (Fig. 1a) and is exposed to high-energy swells generated in the North Atlantic Ocean that are characterised by an annual mean significant wave height (H_s) of about 1.36 m and a mean period (T_m) of the order of 6.5 s (Butel et al., 2002). Tides range from 1.5 m to 4.8 m with an average of about 3.2 m.

During the Biscarrosse field experiment carried out in June 2007 (Bruneau et al., 2009), the beach exhibited a relatively alongshore-uniform subtidal outer bar and a well-developed inner bar-and-rip morphology with a wide range of wavelengths (Fig. 1b). A well-developed bar and rip system (narrow and deep rip channel, Fig. 1b) was intensively instrumented to investigate the time evolution of wave-driven circulation. Persistent shore-normal waves were measured during the experiment with offshore significant wave heights ranging from 0.6 to 3 m and peak periods ranging from 8 to 11 s. A detailed description of the field site and measured wave-driven circulation during the experiment is given in Bruneau et al. (2009). The authors emphasised the strong tidal modulation of the rip currents for low-energy conditions ($H_s < 1$ m) with a maximum rip flow magnitude between low and mid tides, and reasonably large mean rip current flows (>0.5 m/s). This behaviour differs from the one during energetic conditions when intense undertow dominates the overall rip current circulation throughout the whole tide cycle.

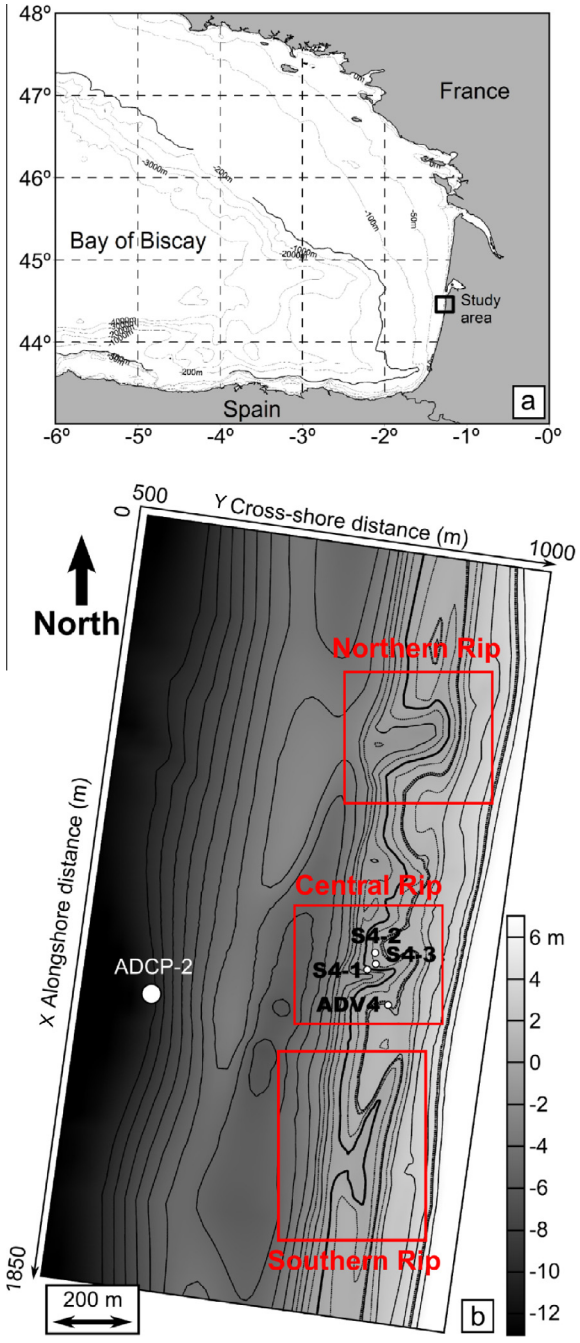

Fig. 1. (a) Atlantic front of the French Coast and continental shelf in the Bay of Biscay. The black box shows the Biscarrosse Beach location; (b) The Biscarrosse double-barred Beach during the field experiment (June 2007) with the deployment positions of the ADCP-2, S4 and the ADV4 sensors. Red squares indicate the three bar/rip morphologies used in the present study. The 0 level refers to the lowest astronomical tide. (For interpretation of the references to colour in this figure caption, the reader is referred to the web version of this article.)

2.2. Numerical model strategy, set-up and application

Our modelling system couples the spectral wave model SWAN (Booij et al., 1999) with the non-linear shallow water circulation model MARS (Lazure and Dumas, 2008) using the depth-averaged (2DH) mode. Recently, wave-related processes were integrated (Bruneau et al., 2008, 2011) to compute wave-driven circulation according to Smith (2006). Defining $\vec{U}$, the horizontal velocity and ζ, the free surface elevation, mass and momentum conservation equations can be derived as follows:

$$\partial_t \bar{\zeta} + \partial_i \bar{h} U_i = -\partial_i \tilde{Q}_i \quad (1)$$

$$\partial_t U_i + U_j \partial_j U_i + g \partial_i \bar{\zeta} = -\partial_i \tilde{J} + \frac{D^r k_i}{\sigma_r \rho \bar{h}} + \frac{\tilde{Q}_j}{\bar{h}}(\partial_i U_j - \partial_j U_i) + \frac{H_i}{\rho \bar{h}} + \frac{\bar{\tau}_i^S - \bar{\tau}_i^B}{\rho \bar{h}} \quad (2)$$

where subscript i refers to the two horizontal coordinates. X and Y represent the alongshore and cross-shore directions, respectively. t is the time, ρ is the water density, g is the gravitational acceleration, $\bar{h}$ is the mean water depth, H_i is the lateral turbulent shear stress, D_r is the roller energy dissipation and, τ_i^S and τ_i^B are the surface and bottom shear stresses, respectively. The wave mass transport is written as:

$$\tilde{Q}_i = (E^w + E^r)\frac{k_i}{\rho c k} \quad (3)$$

where k_i is the wave number, E^w and E^r are the energy induced by the wave-organised motions and the roller contribution, respectively. c_p is the wave phase celerity and σ_r is the relative frequency.

Finally, with the wave group celerity c_g, the non-rotational contribution to radiation stresses J is computed as:

$$\tilde{J} = \frac{E^w}{\rho\bar{h}}\left(\frac{c^g}{c} - \frac{1}{2}\right) + \frac{E^r}{2\rho\bar{h}} \tag{4}$$

The surface and bottom friction are given by:

$$\bar{\tau}_i^S = \rho\ 0.0015\ \|\vec{U}^{Wind}\| U_i^{Wind} \tag{5}$$

$$\bar{\tau}_i^B = \frac{2}{\pi}\rho\ 0.006\ \|\vec{U}^w\| U_i \tag{6}$$

where U^{Wind} is the wind velocity at 10 m and U^w is the wave orbital velocity magnitude.
The mixing term H_i is parameterized as:

$$H_i = \rho\bar{h}\partial_j\left(\nu_t\partial_j U_i\right) \tag{7}$$

where ν_t is the horizontal turbulent eddy viscosity coefficient calculated as:

$$\nu_t = M\bar{h}\left(\frac{D^w}{\rho}\right)^{1/3} + f_v\ 0.01\ \Delta_s^{1.15} \tag{8}$$

where D^w is the wave dissipation due to the breaking, M is a constant set to 2.5, f_v is 6.5 $m^{0.85}/s$ and Δ_s is the grid spacing. More details can be found in Bruneau et al. (2011).

To simulate the circulation during the field campaign, the model was forced along its open boundary by wave directional spectra and water elevations gathered from an ADCP moored by 10-m water depth seaward of the outer bar (ADCP-2 in Fig. 1b). Periodic lateral conditions were applied. A regular grid with 15-m resolution in both directions was used for both the wave and the flow models. This model was successfully validated against Biscarrosse 2007 dataset (Bruneau et al., 2011).

3. Description and analysis of the phenomenon

3.1. Description of the tide-induced asymmetry

Measurements carried out during the Biscarrosse field experiment display a striking asymmetrical behaviour of flow patterns between flood and ebb, as illustrated in Fig. 2b and c. During the two first days of the campaign, the tidal range was almost constant (around 3.7 m – cf. Fig. 2a) with roughly shore-normal low-energy waves (H_s ranging from 0.6 to 1 m – cf. Fig. 2a). Analyzing the distribution of the wave height dependent on the water level (not shown here) demonstrates that there is no correlation between the wave height and the water level (for example no higher waves during the ebb). Fig. 2b shows the 20-min averaged cross-shore currents at the three different locations of the S4 current metre. When deployed near the rip neck (mainly first tide cycle, position $S4-1$ but also near the rip edge during the last cycle, $S4-3$), the S4 measured significant rip currents between 0.4 and 0.8 m/s with ebb currents around 40–60% stronger than flood currents. Between low and mid-tide, for weaker mean currents (0.2 m/s at location S4 – 2), the observed rip current flow is systematically 40 to 90% larger during ebb compared to flood. This asymmetrical behaviour is reasonably well reproduced by the model, although the measurements are local (0.50 m from the bottom), while the modelled velocities are depth-averaged. The analysis of the mean cross-shore currents in the southern feeder flow (ADV4 location in Fig. 2c) reveals an opposite behaviour with 100% stronger onshore currents during flood than during ebb. Thus, it is worth investigating that the influence of tide is not only restricted to variations of water level.

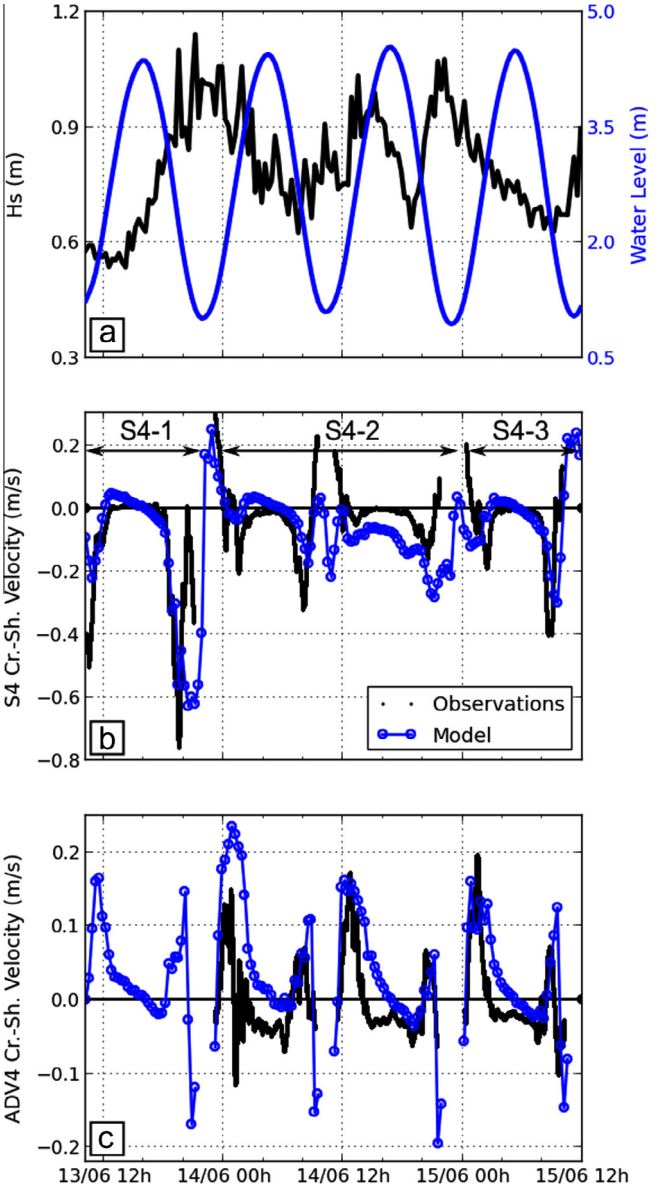

Fig. 2. (a) Significant wave heights (black line) and water levels (blue line); (b) 20 min averaged cross-shore (denoted Cr.-Sh.) currents measured (dark plain line) and modelled (circles and blue line) at the S4 current metre location, deployed near the rip neck; (c) 20-min averaged cross-shore currents measured (dark plain line) and modelled (circles and blue line) at the ADV4 location, deployed in the southern feeder. Offshore (onshore)-directed currents are negative (positive). References $S4-1$ to $S4-3$ indicate the three deployment locations taken by the S4 current metre during the field campaign (cf. Fig. 1b). (For interpretation of the references to colour in this figure caption, the reader is referred to the web version of this article.)

3.2. Origin of the asymmetry

As shown in Fig. 2, the numerical model is able to reproduce the hydrodynamic circulation over a complex, strongly non-uniform morphology with fair accuracy. Flow asymmetries between rising and falling tides for a given water level are well captured. To investigate the influence of both waves and tides on the rip current dynamics, the authors performed numerical simulations considering 3 configurations: (1) tide only, (2) waves with tidal influence restricted to water level variations (i.e. suite of stationary runs) and (3) non-stationary runs with tide and waves. In order to investigate the possible presence of non-linear effects, the results of simulation (3) were compared with the sum of simulations (1) and (2). We applied a simplified tide represented by M2 and a

wave forcing representative of average wave conditions on the Aquitanian coast ($H_s = 1.36$ m, $T_m = 6.5$ s, a 4° incidence from the North and a tidal range of 3.2 m). The location of the maximum rip currents is estimated at each time step for the tide and wave interaction simulation (3). Then the maximum rip speed for configurations 1 and 2 are evaluated at the same locations.

Fig. 3 shows that for configuration (2), the maximum rip flow velocity is similar during ebb and flood. When tide only is considered (configuration 1), currents are offshore-directed during the falling tide and onshore-directed during the rising tide with magnitudes reaching 0.05 m/s close to mid tide. When both tide and waves are considered (configuration 3), the model shows a rip current intensity 20% larger during ebb than during flood. The sum of the currents predicted in configuration (1) and (2) closely matches the currents of configuration (3) during the falling tide but is slightly stronger during the rising tide. This suggests that tide-induced currents are quasi-linearly superimposed on wave-induced currents.

The tide-induced signatures in rip channels seem to originate from the filling of the intertidal volume in the associated channels. To verify this hypothesis, a rough geometric estimate was also performed. First, the surface areas and the cross sections of the three studied rips were empirically delineated and computed (Table 1). Then, the mean tidal range during the field experiment implies vertical variations of the free-surface elevation of the order of 0.00025 m/s at mid-tide. These parameters yield mean currents ranging from 0.05 to 0.06 m/s for the three studied rips (Table 1). Although this estimate is very rough and over-simplifies the circulation that occurs in reality, the current velocities obtained are of the same order of magnitude as those computed with our numerical model.

3.3. Importance of tidal range vs wave conditions

In order to investigate the respective contributions of wave conditions and tidal range (TR) to rip-current flow asymmetry, a set of 30 additional simulations were performed for various combinations of these parameters (5 TR, 3 H_s and 2 T_m). TR was varied from 1.5 to 4.5 m, which corresponds to the range of TR observed at Biscarosse. Significant wave heights were varied from 0.5 to 2.5 m and mean wave periods were set to 6.5 s or 11 s, which is once again in line with the local wave climate (Butel et al., 2002). Wave heights larger than 2.5 m were not considered as under such conditions, wave breaking occurs on the outer bar with wave-driven circulation on the inner bar increasingly influenced by breaker patterns across the outer bar. To verify that the observed tide-induced asymmetry is not specific to the instrumented rip-channel, we extended this analysis to the two other rip channels located within the computational domain (Fig. 1b).

As the maximum rip current never occurs at the same water level between the falling and rising tide, the following methodology was chosen to characterise the asymmetry. Using the time series of maximum rip current as detailed in Section 3.2 and Fig. 3, the offshore currents are integrated over the ebb and flood tide phase, denoted V_{Ebb} and V_{Flood}, respectively. Then a classical formulation is used:

$$Asymmetry(\%) = 100\frac{V_{Ebb} - V_{Flood}}{(V_{Ebb} + V_{Flood})/2} \quad (9)$$

The synthesis of the 30 simulations is presented in Fig. 4. This figure illustrates the intensity of the asymmetry (colourbar) function of the tide range; the rip current peak velocity is also given to provide information on the rip current activity. Results clearly show that tide-induced asymmetry increases with increasing tidal range for all wave conditions and all the rip current systems considered. This analysis also reveals that the asymmetry is weak (<5%) for a 1.5 m tidal range (microtidal conditions) and increases quite linearly up to 45% for TR = 4.5 m (Fig. 4c). Fig. 4 also shows an increase in tide-induced asymmetry with decreasing incident wave height. The case H_s = 0.5 m shows very strong asymmetries

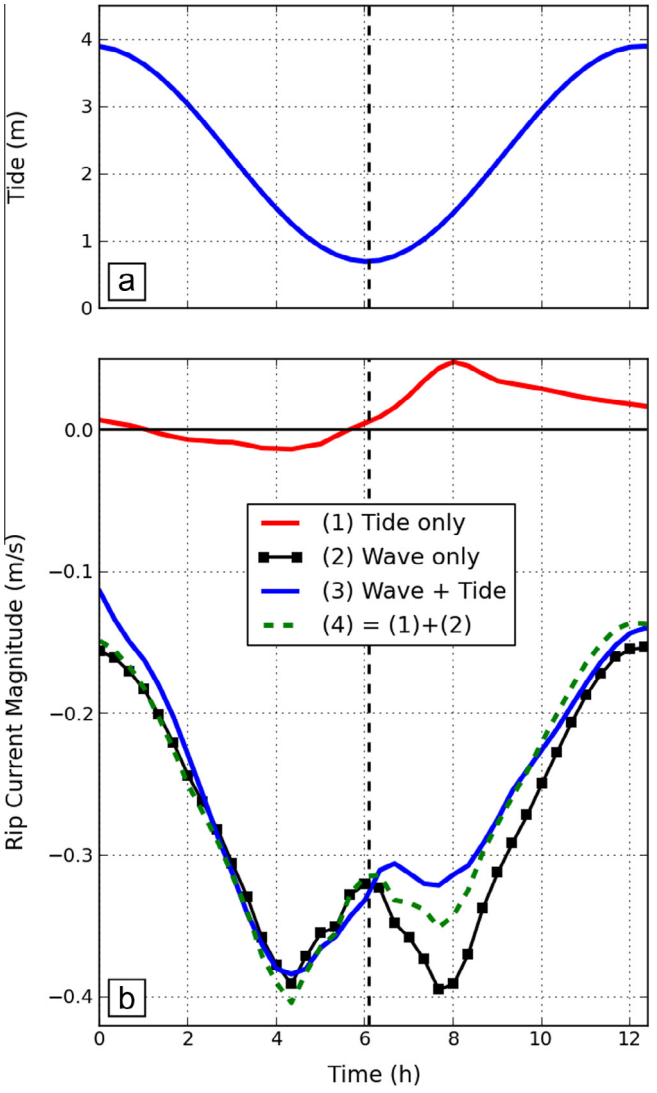

Fig. 3. (a) water level – tide restricted to M2; (b) time series of the "maximum" rip current velocity for each configurations: (1) tide only, (2) waves with tidal influence restricted to water level variations, (3) non-stationary runs with tides and waves and (4) the sum of simulation (1) and (2). A representative forcing of the Aquitanian coast was used: $H_s = 1.36$ m, $T_m = 6.5$ s, 4° incidence from the North and a tidal range of 3.2 m.

Table 1
Geometric parameters of the three studied rips and mean resulting velocity at mid-tide.

	Rip-channel surface area (m^2) at mid-tide	Rip-channel cross-section (m^2) at mid-tide	Resulting mean velocity at mid-tide (m/s)
Northern rip	85,000	330	0.06
Central rip	50,000	200	0.06
Southern rip	85,000	400	0.05

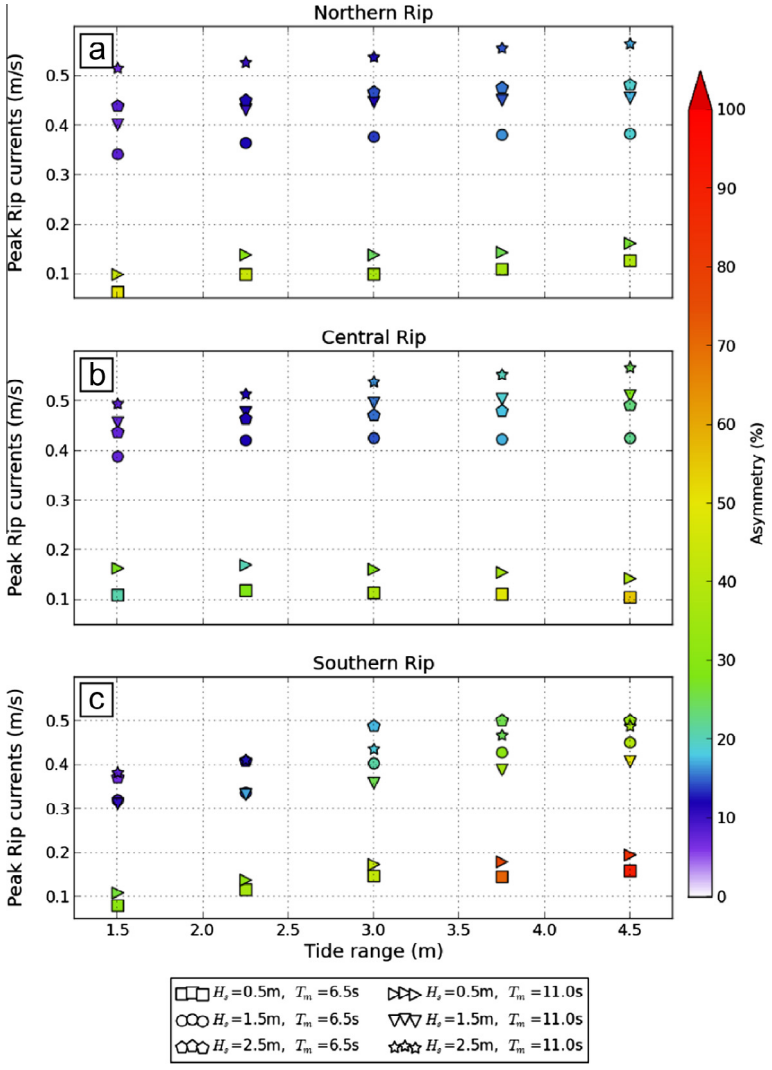

Fig. 4. Maximum rip current intensities dependent on the tide range for the set of 30 simulations superimposed with the asymmetry magnitude (cf. colourbar for intensity) of the rip currents between ebb and flood for each of the three bar/rip morphologies (a–c). The different symbols represent different shore-normal wave forcing (varying significant wave height and mean period).

(reaching 100%) although the maximum rip currents are very weak (between 0.1 and 0.2 m/s). The comparison for contrasting rip morphologies also suggests that rip channel morphology has a significant impact on the asymmetry. The Northern rip current associated with a deep and large channel displays weaker asymmetry (5–20%) while the Southern rip, narrower and with two long feeder channels, shows a stronger asymmetry reaching 45%.

4. Discussion

4.1. Hydro-geomorphic setting promoting tide-induced asymmetries in rip currents

The present study demonstrates and quantifies for the first time the importance of tidal currents on a wave-dominated rip-channelled beach located in a meso-macrotidal environment. Both observations and model results show a strong asymmetry of rip current magnitude, with stronger velocities during ebb compared with flood. This asymmetry is the strongest between low and mid tide when both rip activity and the rate of change in tidal elevation are the strongest. Numerical experiments show a weak asymmetry (<5%) for small tidal ranges because tidal water level variations are too slow to induce significant tidal currents. This explains why asymmetries in rip currents have never been reported in micro tidal environment (e.g. MacMahan et al., 2005, 2006, 2008; Reniers et al., 2007).

Conversely, one could expect very large asymmetries in macrotidal environments, such as in Perranporth, England (e.g. Scott et al., 2009; Austin et al., 2010). Surprisingly enough, these studies have never reported significant asymmetries in rip current magnitude. While net tidal currents are observed by Austin et al. (2013) in the alongshore-directed flows, no clear asymmetry was noticed in the measurements. A possible explanation may be that rip channels at Perranporth are observed in the lower part of the beach profile, are strongly extended in the alongshore direction and are only active either side of low tide, i.e. when tide-induced water level variations are slow. The peak of rip currents (cross-shore velocities) and tide flows (alongshore currents), in Fig. 4 of Austin et al. (2013) are noticeably shifted. However, the presence of asymmetry should be verified under energetic wave conditions, where rip channels may be active around mid-tide as well as in headland rip settings that, conversely to open beach rips, do not occur systematically for low water levels (Castelle and Coco, 2013).

4.2. Implications for sediment dynamics and beach safety

Sediment transport in the nearshore is a function of current velocity at a power typically ranging from 3 to 5. The results presented in this study reveal rip currents typically 20 to 45% stronger during ebb than during flood. Sediment transport that takes place in rip channels at ebb would thus be up almost one order of magnitude larger compared to flood. This behaviour has the potential to impact the bar/rip system morphodynamics. Existing numerical studies have succeeded in reproducing the finite-amplitude dynamics of bar/rip morphologies using a stationary approach (i.e. no tidal current generation, e.g. Garnier et al., 2008; Castelle et al., 2012) with bedform lengthscales and overall patterns mimicking those in the field. In addition, bar and rip morphologies on microtidal and meso-macrotidal beaches are essentially similar in patterns. Yet, accounting for tide-induced currents in such numerical exercises will allow in-depth exploration of the role of tide on rip channel morphodynamics in meso-macrotidal settings as well as the modulation of the bedform growth, decay and migration by tidal currents.

Around 80% of the drowning accidents around the world are due to rip current hazards (http://www.ceoe.udel.edu/ripcurrents/safety/index.html, Carey et al., 2006). Our results have strong implications for beach safety since they suggest that rip currents may be more dangerous at ebb than flood. This hypothesis is corroborated by lifeguards' experience on the Aquitanian Coast (personal communication) but will have to be investigated further. Rip current hazard depends on rip velocity, but also on the ability of the rip to flush out floating material from the surf zone into the inner shelf region (Castelle and Coco, 2013). Surf zone retention of rip current systems so far has been addressed on micro-tidal beaches (e.g., Reniers et al., 2009). The impact of tide-induced currents on the surf zone flushing by rips should be explored further.

4.3. Conclusions and future works

This study reveals 20 to 45% stronger rip currents during ebb than during flood on a rip-channelled beach located in a meso-macrotidal environment. This behaviour is explained by the superimposition of tidal currents onto wave-induced currents. Numerical experiments show that tidal currents are almost linearly superimposed on wave-induced currents and rip current asymmetry grows linearly as a function of the tide range. This phenomenon has potential implications for sediment transport, beach morphodynamics and also beach safety. Such tidally-induced asymmetries have never been reported before. Further field investigations should be conducted on other meso- to macrotidal sites to further investigate this phenomenon and provide a more generic description.

Acknowledgements

This Biscarrosse 2007 campaign was carried out thanks to the financial support of the BRGM. This study was performed within the framework of the ECORS (SHOM) Project and the MODLIT (SHOM and INSU) Project that have also sponsored this study. The authors thank the French Navy (SHOM) for the large bathymetry survey carried out on the studied field that was required for such an experiment. They are also grateful to the teams and students involved in the field experiment. The authors thank the developers of the models SWAN and MARS. This work was partially funded by a postdoctoral research Grant to the first author from the Fundação para a Ciência (SFRH/BPD/67041/2009). Xavier Bertin was funded by Project ANR JC DYNAMO (agreement ANR-12-JS02–00008-01) and Bruno Castelle by Project BARBEC (ANR N2010 JCJC 602 01).

References

Austin, M., Scott, T., Brown, J., Brown, J., MacMahan, J., Masselink, G., Russell, P., 2010. Temporal observations of rip current circulation on a macro-tidal beach. Cont. Shelf Res. 30, 1149–1165. http://dx.doi.org/10.1016/j.csr.2010.03.005.

Austin, M., Scott, T., Masselink, G., Russell, P., 2013. Rip current prediction: development, validation and evaluation of an operational tool. J. Coastal Res., 0749-0208 29, 283–300. http://dx.doi.org/10.2112/JCOASTRES-D-12-00093.1.

Bonneton, P., Bruneau, N., Castelle, B., Marche, F., 2010. Large scale vorticity generation due to dissipating waves in the surf zone. Discrete Contin. Dyn. Syst. – Ser. B 13, 729–738. http://dx.doi.org/10.3934/dcdsb.2010.13.729.

Booij, N., Ris, R.C., Holthuijsen, L., 1999. A third-generation wave model for coastal regions 1. Model description and validation. J. Geophys. Res. 104, 7649–7666.

Brander, R.W., 1999. Field observations on the morphodynamic evolution of low wave energy rip current system. Mar. Geol. 157, 199–217.

Brander, R.W., Short, A.D., 2000. Morphodynamics of a large-scale rip current system at Muriwai Beach, New Zealand. Mar. Geol. 165, 27–39.

Bruneau, N., Bonneton, P., Castelle, B., Pedreros, R., 2011. Modeling rip current circulations and vorticity in a high-energy mesotidal-macrotidal environment. J. Geophys. Res. – Oceans 116. http://dx.doi.org/10.1029/2010JC006693.

Bruneau, N., Castelle, B., Bonneton, P., Pedreros, R., Almar, R., Bonneton, N., Bretel, P., Parisot, J., Sénéchal, N., 2009. Field observations of an evolving rip current on a meso-macrotidal well-developed inner bar and rip morphology. Cont. Shelf Res. 29, 1650–1662. http://dx.doi.org/10.1016/j.csr.2009.05.005.

Bruneau, N., Castelle, B., Bonneton, P., Pedreros, R., Parisot, J.P., Sénéchal, N., 2008. Modelling of high-energy rip current during Biscarrosse field experiment. In: 31st International Conference on Coastal Engineering (ICCE 2008), Hamburg, Germany, pp. 901–913. http://dx.doi.org/10.1142/97898142774260076.

Butel, R., Dupuis, H., Bonneton, P., 2002. Spatial variability of wave conditions on the French Aquitanian Coast using in-situ data. J. Coastal Res. 36, 96–108.

Carey, W., Mosher, K., Rogers, S., 2006. Rip current safety and public awareness – the beach vacation as an education destination. J. Mar. Educ. 22.

Castelle, B., Bonneton, P., Dupuis, H., Sénéchal, N., 2007. Double bar beach dynamics on the high-energy meso-macrotidal French Aquitanian Coast: a review. Mar. Geol. 245, 141–159.

Castelle, B., Bonneton, P., Sénéchal, N., Dupuis, H., Butel, R., Michel, D., 2006. Dynamics of wave-induced currents over an alongshore non-uniform multiple-barred sandy beach on the Aquitanian Coast, France. Cont. Shelf Res. 26, 113–131.

Castelle, B., Coco, G., 2013. Surf zone flushing on embayed beaches. Geophys. Res. Lett. 40, 1–5. http://dx.doi.org/10.1002/grl.50485.

Castelle, B., Marieu, V.G.C., Bonneton, P., Ruessink, B., 2012. On the impact of an offshore bathymetric anomaly on surfzone rip channels. J. Geophys. Res. – Earth Surf. 117.

Castelle, B., Michallet, H., Marieu, V., Leckler, F., Dubardier, J., Lambert, A., Berni, C., Bonneton, P., Barthélemy, E., Bouchette, F., 2010. Laboratory experiment on rip current circulations over a moveable bed: drifter measurements. J. Geophys. Res. – Oceans 115. http://dx.doi.org/10.1029/2010JC006343.

Garnier, R., Bonneton, P., Falqués, A., Calvete, D., 2008. Modelling the formation and the nonlinear evolution of crescentic bars of the aquitanian coast. La Houille Blanche 03. http://dx.doi.org/10.1051/lhb:2008024, Proceedings of the Génie Côtier, Génie Civil Conference 2006, Brest, France.

Haller, M.C., Dalrymple, R.A., 2001. Rip currents instabilities. J. Fluid Mech. 433, 161–192.

Holman, R.A., Symonds, G., Thornton, E.B., Ranasinghe, R., 2006. Rip spacing and persistence on an embayed beach. J. Geophys. Res. 111.

Kennedy, A., Thomas, D., 2004. Drifter measurements in a laboratory rip current. J. Geophys. Res. – Oceans 109. http://dx.doi.org/10.1029/2003JC001927.

Lazure, P., Dumas, F., 2008. An external-internal mode coupling for a 3d hydrodynamical model for applications at regional scale (mars). Adv. Water Resour. 21, 233–250. http://dx.doi.org/10.1016/j.advwatres.2007.06.010.

MacMahan, J., Thornton, E., Reniers, A., Stanton, T., Symonds, G., 2008. Low-energy rip currents associated with small bathymetric variations. Mar. Geol. 255, 156–164.

MacMahan, J.H., Reniers, A.J.H.M., Thornton, E.B., Stanton, T.P., 2004a. Infragravity rip current pulsations. J. Geophys. Res. 109, 1–9.

MacMahan, J.H., Reniers, A.J.H.M., Thornton, E.B., Stanton, T.P., 2004b. Surf zone eddies coupled with rip current morphology. J. Geophys. Res. 109. http://dx.doi.org/10.1029/2003JC002083.

MacMahan, J.H., Thornton, E.B., Reniers, A.J.H.M., 2006. Rip current review. Coastal Eng. 53, 191–208.

MacMahan, J.H., Thornton, E.B., Stanton, T.P., Reniers, A.J.H.M., 2005. Ripex – rip currents on a shore-connected shoal beach. Mar. Geol. 218, 113–134.

Reniers, A.J.H.M., MacMahan, J.H., Beron-Vera, F.J., Olascoaga, M.J., 2010. Rip-current pulses tied to lagrangian coherent structures. Geophys. Res. Lett. 37. http://dx.doi.org/10.1029/2009GL041443.

Reniers, A.J.H.M., MacMahan, J.H., Thornton, E.B., Stanton, T.P., 2007. Modeling of very low frequency motions during ripex. J. Geophys. Res. 112. http://dx.doi.org/10.1029/2005JC003122.

Reniers, A.J.H.M., MacMahan, J.H., Thornton, E.B., Stanton, T.P., Henriquez, M., Brown, J.W., Brown, J.A., Gallagher, E., 2009. Surf zone surface retention on a rip?channeled beach. J. Geophys. Res. 114. http://dx.doi.org/10.1029/2008JC005153.

Scott, T., Masselink, G., Russell, P., Austin, M., Wills, S., Wooler, A., 2011. Rip current hazards on large-tidal beaches in the UK. In: Leatherman, S., Fletemeyer, J. (Eds.), Rip Currents: Beach Safety, Physical Oceanography, and Wave Modeling. CRC Press, pp. 225–243. http://dx.doi.org/10.1201/b10916-15.

Scott, T., Russell, P., Masselink, G., Wooler, A., 2009. Rip current variability and hazard along a macrotidal coast. J. Coastal Res., SI56, 895–899. (Proceedings of the 10th International Coastal Symposium, Lisbon, Portugal, ISSN 0749–0258).

Shanks, A.L., Morgan, S.G., MacMahan, J.H., Reniers, A.J.H.M., 2010. Surf zone physical and morphological regime as determinants of temporal and spatial variation in larval recruitment. J. Exp. Mar. Biol. Ecol. 392, 140–150. http://dx.doi.org/10.1016/j.jembe.2010.04.018.

Smith, J., 2006. Wave-current interactions in finite depth. J. Phys. Oceanogr. 36, 1403–1419.

Turner, I.L., Whyte, D., Ruessink, B.G., Ranasinghe, R., 2007. Observations of rip spacing, persistence and mobility at a long, straight coastline. Mar. Geol. 236, 209–221.